PCCP

COMMUNICATION

View Article Online
View Journal | View Issue

Cite this: *Phys. Chem. Chem. Phys.*, 2016, **18**, 14186

Received 12th April 2016,
Accepted 5th May 2016

DOI: 10.1039/c6cp02369j

www.rsc.org/pccp

Endohedral charge-transfer complex $Ca@B_{37}^-$: stabilization of a B_{37}^{3-} borospherene trianion by metal-encapsulation†

Qiang Chen,[ab] Hai-Ru Li,[a] Wen-Juan Tian,[a] Hai-Gang Lu,*[a] Hua-Jin Zhai*[a] and Si-Dian Li*[a]

Based on extensive first-principles theory calculations, we present the possibility of an endohedral charge-transfer complex, C_s $Ca@B_{37}^-$ (I), which contains a 3D aromatic fullerene-like C_s B_{37}^{3-} (II) trianion composed of interwoven boron double chains with twelve delocalized multicenter π bonds (12 *mc*–2e π, *m* = 5, 6) over a σ skeleton, completing the B_n^q borospherene family ($q = n - 40$) in the size range of n = 36–42.

Fullerene-like elemental clusters have received great attention in chemistry and materials science ever since the discovery of C_{60} in the gas phase in 1985[1] which opened the gate to the nowadays popular carbon nanotubes[2] and graphenes.[3] However, only a handful of free-standing cage-like elemental clusters had been experimentally characterized before 2014, including the truncated cage-like Au_{16}^-,[4] stannaspherene Sn_{12}^{2-},[5] and plumbaspherene Pb_{12}^{2-}.[6] As the lighter neighbour of carbon in the periodic table, boron is a typical electron-deficient element characterized by multicenter-two-electron (*mc*–2e) bonds in both polyhedral molecules and bulk allotropes.[7] In contrast to boron solids, however, small boron clusters $B_n^{-/0}$ have been experimentally confirmed to be planar or quasi-planar in an unexpectedly wide range of sizes (n = 3–25, 27, 30, 35, 36), unveiling a flat world of boron in close analogy with polycyclic hydrocarbons.[8–20] All-boron fullerenes were not considered before the proposal of the perfect cage-like B_{80} in 2007 which was constructed from C_{60} by capping the twenty surface hexagons.[21] However, B_{80} was later found to strongly favour core–shell structures at various theoretical levels.[22,23] The first all-boron fullerenes D_{2d} $B_{40}^{-/0}$, dubbed borospherenes in the literature, were discovered in the gas phase in 2014 by Zhai and coworkers in a combined experimental and computational study,[24] marking the onset of borospherene chemistry. The cubic-box-like D_{2d} $B_{40}^{-/0}$ are composed of twelve interwoven boron double chains (BDCs) with two B_6 surface hexagons on the top and at the bottom and four B_7 surface heptagons on the waist. Although D_{2d} B_{40}^- is slightly less stable than the quasi-planar global minimum (GM) C_s B_{40}^- of the monoanion, neutral D_{2d} B_{40} proves to be the well-defined GM of the system with a huge energy gap of 3.13 eV between its highest occupied molecular orbital (HOMO) and lowest unoccupied molecular orbital (LUMO) which is comparable with the corresponding value (3.02 eV) of C_{60} using density functional theory (DFT).[24] Furthermore, detailed orbital analyses indicate that D_{2d} B_{40} possesses 12 delocalized π bonds over a σ skeleton made of 48 3c–2e σ bonds, giving three-dimensional (3D) aromaticity to this cage-like molecule. Both endohedral M@B_{40} (M = Ca, Sr) and exohedral M&B_{40} (M = Be, Mg) metalloborospherenes were computationally predicted by Bai *et al.* shortly after.[25] The first axially chiral borospherenes C_3/C_2 B_{39}^- were observed by Chen *et al.* in 2015,[26] presenting the possibility of boron nanotubes composed of interwoven BDCs with helix chirality. In a series of recent investigations based on extensive structural searches and first-principles theory calculations, Chen and coworkers also presented the possibilities of bare C_1 B_{41}^+ and C_2 B_{42}^{2+} (ref. 27) and metal-stabilized C_3/C_2 $Ca@B_{39}^+$,[28] C_s $Ca@B_{38}$,[29] D_{2h} $Li_4\&B_{36}$, C_{2v} $Li_5\&B_{36}^+$, T_h $Li_6\&B_{36}^{2+}$, D_{2h} $Li_2\&[Ca@B_{36}]$, C_{2v} $Li_3\&[Ca@B_{36}]^+$, and D_{2h} $Li_4\&[Ca@B_{36}]^{2+}$,[30] establishing a B_n^q borospherene family ($q = n - 40$, n = 36, 38, 39, 40, 41, and 42) in the size range of n = 36–42.[24–30] The reported B_n^q ($q = n - 40$) borospherenes T_h B_{36}^{4-}, C_s B_{38}^{2-}, C_3/C_2 B_{39}^-, D_{2d} $B_{40}^{-/0}$, C_1 B_{41}^+, and C_2 B_{42}^{2+} all appear to be boron analogues of cubane (C_8H_8). They are all composed of twelve interwoven BDCs with six B_6 hexagonal or B_7 heptagonal faces and possess twelve delocalized multicenter π bonds (*mc*–2e π, *m* = 4, 5, 6) over a σ skeleton made of n + 8 σ bonds. However, whether a fullerene-like B_{37}^{3-} (n = 37 and q = −3) or its derivatives exist or not, still remains unknown to date in both theory and experiments. The latest development in boron clusters is the observation of the seashell-like C_2 $B_{28}^{-/0}$ which, as the smallest borospherene characterized to date in a structural pattern different from D_{2d} B_{40}, possesses one surface hexagon and two surface heptagons.[31] Theoretical predictions

[a] *Nanocluster Laboratory, Institute of Molecular Science, Shanxi University, Taiyuan 030006, China. E-mail: luhg@sxu.edu.cn, hj.zhai@sxu.edu.cn, lisidian@sxu.edu.cn*

[b] *Institute of Materials Science and Department of Chemistry, Xinzhou Teachers' University, Xinzhou 034000, China*

† Electronic supplementary information (ESI) available. See DOI: 10.1039/c6cp02369j

on B_{44} and B_{42}^{+} with octagonal rings or even nonagonal rings have also been reported.[32,33] Two-dimensional (2D) borophene polymorphs, with or without vacancies deposited on Ag(111) substrates, were experimentally synthesized very recently,[34,35] expanding boron nanostructures from planar, tubular, and cage-like clusters to 2D monolayer nanosheets.

In this contribution, based on extensive structural searches and first-principles theory calculations, we present the possibility of an endohedral charge-transfer metalloborospherene C_s $Ca@B_{37}^{-}$ (**I**) which, as the lowest-lying isomer of the monoanion obtained, contains a 3D aromatic fullerene-like C_s B_{37}^{3-} (**II**) trianion composed of 12 interwoven BDCs with 12 delocalized multicenter π bonds over a σ skeleton, extending the B_n^q borospherene family ($q = n - 40$) from n = 36, 38, 39, 40, 41, and 42 to include n = 37. The infrared (IR), Raman and photoelectron spectroscopy (PES) spectra of $Ca@B_{37}^{-}$ (**I**) are computationally simulated to facilitate its future experimental characterization. Other alkaline-earth-metal-stabilized endohedral complexes C_s $M@B_{37}^{-}$ (M = Mg, Sr) similar to $Ca@B_{37}^{-}$ (**I**) are also predicted to be the true minima of the systems.

Extensive minima hopping (MH) structural searches at the DFT level[23,36] were performed on CaB_{37}^{-}, in combination with manually constructed initial structures based on known low-lying isomers of Li_2CaB_{36},[30] B_{38}^{2-}, and CaB_{38}.[29] Full structural optimization and frequency analyses at the hybrid DFT-PBE0 level[37] with the basis set of 6-311+G(d)[38] were performed using the Gaussian 09 suite,[39] with the twenty lowest-lying isomers obtained shown in Fig. 1 and Fig. S1 in the ESI.† The relative stabilities of the five lowest-lying isomers of CaB_{37}^{-} were further refined using the more accurate coupled cluster method with triple excitations (CCSD(T))[40–42] implemented in MOLPRO[43] with the 6-311G(d) basis set at the PBE0 geometries. Natural atomic charges and electronic configurations were analyzed using the NBO 5.0 program[44] and bonding orbital analyses performed using the adaptive natural density partitioning (AdNDP) procedure.[45] The nucleus-independent chemical shift (NICS)[46] at the cage centre was calculated for C_s B_{37}^{3-} (**II**) to assess the 3D aromaticity of the borospherene trianion.

Metal-encapsulation has proven to be an effective approach to stabilize various borospherene anions including B_{36}^{4-} in Li_2&[Ca@B_{36}],[30] B_{38}^{2-} in $Ca@B_{38}$,[29] and B_{39}^{-} in $Ca@B_{39}^{+}$.[28] The same strategy applies to CaB_{37}^{-} which turns out to have the lowest-lying isomer of endohedral C_s $Ca@B_{37}^{-}$ (**I**). As a true minimum of the monoanion with the smallest vibration frequency of ν_{min} = 103.1 cm^{-1}, $Ca@B_{37}^{-}$ (**I**) was generated during an MH structural search starting from a C_1 $Ca@B_{37}^{-}$ constructed by removing one B atom from the previously reported C_s $Ca@B_{38}$.[29] It is composed of twelve interwoven BDCs, with two B_5 surface pentagons, one B_6 surface hexagon, and three B_7 surface heptagons in an overall symmetry of C_s. It can also be viewed as a distorted cubic-box made of six apex-sharing and two corner-overlapping quasiplanar B_6 triangles (Fig. 1 and Table S1, ESI†). It is the first stable endohedral metalloborospherene reported to date with pentagonal holes on the cage surface.[24,26–30] $Ca@B_{37}^{-}$ (**I**) is highly stable with a huge negative formation energy of −589.6 kcal mol^{-1} with respect to B_{37}^{3-} (**II**) + Ca^{2+} = $Ca@B_{37}^{-}$ (**I**). The second lowest-lying isomer C_1 $Ca@B_{37}^{-}$ (**2**), which can be obtained by a slight twist of C_s $Ca@B_{37}^{-}$ (**I**) (Fig. S1, ESI†), lies only 0.07 eV and 0.05 eV higher than the latter with zero-point-corrections included at the CCSD(T) and PBE0 levels, respectively. The third lowest-lying C_1 $Ca@B_{37}^{-}$ (**3**), which is 0.25 eV less stable than $Ca@B_{37}^{-}$ (**I**) at the CCSD(T) level, can be produced from the previously reported C_s $Ca@B_{38}$[29] by removing one B atom; it possesses four B_6 hexagons and two B_7 heptagons on the surface, with a tetracoordinate defect site between one heptagon and its neighbouring hexagon. The fourth lowest-lying C_1 $Ca@B_{37}^{-}$ (**4**), a positional isomer of the third isomer (Fig. S1, ESI†), lies 0.31 eV higher than $Ca@B_{37}^{-}$ (**I**) and possesses a tetracoordinate defect site between the two neighbouring surface heptagons. The fifth lowest-lying high-symmetry C_{2v} $Ca@B_{37}^{-}$ (**5**), which lies 0.63 eV higher than $Ca@B_{37}^{-}$ (**I**), can be obtained from T_h $Ca@B_{36}^{2-}$ (ref. 30) by adding a face-capping B atom over the surface hexagon at the bottom. The endohedral C_1 $Ca@B_{37}^{-}$, composed of twelve BDCs with one heptagon and five hexagons constructed from T_h B_{36}^{4-}, is automatically converted to the second isomer C_1 $Ca@B_{37}^{-}$ during structural optimization due to strong strain between the heptagon and its neighbouring hexagons. Quasi-planar isomers of CaB_{37}^{-} with one or two adjacent hexagonal holes constructed from B_{35}^{-} and B_{36}[18,19] turn out to be at least 0.54 eV less stable than $Ca@B_{37}^{-}$ (**I**) at the PBE0 level (Fig. S1, ESI†). Extensive MH global searches for CaB_{37}^{-}, with over 1300 stationary points on the potential surface probed, generated no isomers with lower energies than $Ca@B_{37}^{-}$ (**I**). We notice that all the twelve lowest-lying isomers of CaB_{37}^{-} obtained (**1–9**) possess 3D endohedral structures (Fig. S1, ESI†). More interestingly, the lowest-lying C_s $Ca@B_{37}^{-}$ (**I**) contains a fullerene-like C_s B_{37}^{3-} (**II**) which is a true minimum of the trianion with the smallest vibrational frequency of ν_{min} = 156.8 cm^{-1}, completing the B_n^q borospherene family in the size range between n = 36–42.[24,26–30] Endohedral metalloborospherenes C_s $Mg@B_{37}^{-}$ and C_s $Sr@B_{37}^{-}$, similar to $Ca@B_{37}^{-}$ (**I**), also appear to be the true minima of the systems. Initial calculations at the PBE0 level indicate that $Ca@B_{37}^{-}$ (**I**) can be further stabilized by capping a heptagon on the cage surface with an η^7-Li^+ monocation to form the closed-shell neutral C_s Li&[Ca@B_{37}] or C_1 Li&[Ca@B_{37}] which are practically isoenergetic species with HOMO–LUMO gaps of 1.91 eV and 2.03 eV, respectively. Neutral Li&[Ca@B_{37}] salts with both an

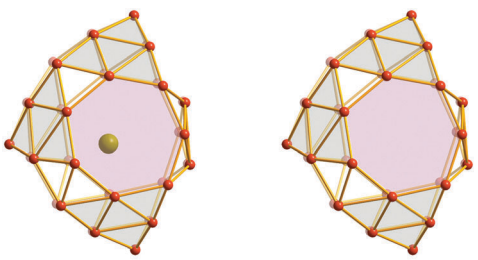

I C_s $Ca@B_{37}^{-}$ (^{1}A′) **II** C_s B_{37}^{3-} (^{1}A′)

Fig. 1 Optimized structures of C_s $Ca@B_{37}^{-}$ (**I**) and C_s B_{37}^{3-} (**II**), with the quasiplanar B_6 triangles at the corners highlighted in grey.

encapsulated Ca^{2+} and a face-capping Li^{+} may exist in B–Ca–Li ternary solids.

The high stability of $Ca@B_{37}^{-}$ (**I**) originates from its unique electronic structure and bonding pattern. Natural bonding orbital (NBO) analyses show that $Ca^{2+}@B_{37}^{3-}$ (**I**) is a typical charge-transfer complex with the encapsulated Ca ($[Ar]4s^2$) donating two 4s electrons to the B_{37} cage, as indicated by the calculated natural atomic charges of q_{Ca} = +1.71 $|e|$ and the atomic electronic configurations of Ca $[Ar]4s^{0.12}3d^{0.17}$ in it. Weak d–p coordination interactions between the Ca^{2+} centre and the B_{37}^{3-} ligand may also contribute to stabilize the complex. The closed-shell $Ca@B_{37}^{-}$ (**I**) and B_{37}^{3-} (**II**) possess large calculated HOMO–LUMO energy gaps of 1.94 eV and 1.96 eV, respectively, which are comparable with (though smaller than) the corresponding values of 2.98, 2.70, 2.89, 3.13, 3.16, 3.24, and 3.02 eV obtained for D_{2h} $Li_4\&B_{36}$, C_s CaB_{38}, C_3 B_{39}^{-}, D_{2d} B_{40}, C_1 B_{41}^{+}, C_2 B_{42}^{2+}, and I_h C_{60} at the same theoretical level, respectively.[24,26–30]

Detailed AdNDP[45] analyses unveil the bonding patterns of isovalent $Ca@B_{37}^{-}$ (**I**) and B_{37}^{3-} (**II**). As shown in Fig. 2, bare C_s B_{37}^{3-} (**II**) possesses 2 2c–2e σ bonds at the bottom of the two surface pentagons and 37 delocalized 3c–2e σ bonds on the 37 B_3 surface triangles with occupation numbers |ON| = 1.78–1.97 $|e|$, and 6 delocalized 6c–2e σ bonds on the 6 quasi-planar B_6 triangles with |ON| = 1.91–1.95 $|e|$. As the central B_3 triangles make major contributions to the 6c–2e σ bonds, the delocalized σ interactions can be approximately treated as 43 3c–2e σ bonds with one σ bond on each surface B_3 triangle. The remaining 24 valence electrons are distributed in 12 delocalized *m*c–2e π bonds (*m* = 5, 6) with |ON| = 1.88–1.95 $|e|$ over the σ skeleton made of 45 σ bonds, including 7 5c–2e π bonds and 5 6c–2e π bonds (Fig. 2). With 12 delocalized π bonds over the 12 interwoven BDCs, B_{37}^{3-} (**II**) is π-isovalent with the borospherenes T_h B_{36}^{4-}, C_s B_{38}^{2-}, C_3/C_2 B_{39}^{-}, D_{2d} $B_{40}^{-/0}$, C_1 B_{41}^{+}, and C_2 B_{42}^{2+} reported so far,[24,26–30] completing the B_n^q series ($q = n - 40$) in the size range of n = 36–42. Such a bonding pattern renders 3D aromaticity to C_s B_{37}^{3-} (**II**), as indicated by a calculated NICS value of −33.2 ppm at the cage centre which is comparable with the corresponding values of −36 ppm, −37 ppm, −38 ppm, −39 ppm, −43 ppm, −41 ppm, and −40 ppm calculated for T_h B_{36}^{4-}, C_s B_{38}^{2-}, C_3 B_{39}^{-}, C_2 B_{39}^{-}, D_{2d} B_{40}, C_1 B_{41}^{+}, and C_2 B_{42}^{2+}, respectively.[24,26–30] As demonstrated in Fig. 2, the metal-stabilized C_s $Ca@B_{37}^{-}$ (**I**) possesses the same σ and π bonding patterns as C_s B_{37}^{3-} (**II**), with 12 delocalized *m*c–2e π bonds (*m* = 5, 6) over a σ skeleton composed of 45 σ bonds. Neutral Li&[$Ca@B_{37}$] with a face-capping η^7-Li^{+} monocation also has similar σ and π bonding patterns with $Ca@B_{37}^{-}$ (**I**) and B_{37}^{3-} (**II**). The Ca atom encapsulated in the metalloborospherenes contributes two 4s electrons to facilitate the formation of the delocalized π-system.

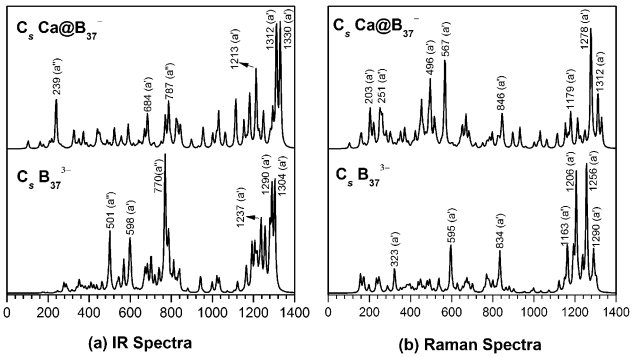

Fig. 3 Simulated IR (a) and Raman spectra (b) of C_s $Ca@B_{37}^{-}$ (**I**) compared with that of C_s B_{37}^{3-} (**II**) at the PBE0 level.

We calculate the vibrational frequencies and simulate the IR and Raman spectra of $Ca^{2+}@B_{37}^{3-}$ (**I**) and B_{37}^{3-} (**II**) in Fig. 3 to facilitate their future spectroscopic characterization. As expected, these cage-like-B_{37}^{3-}-based species exhibit similar IR and Raman spectra. The major IR bands around 1304 cm^{-1} (a′ mode), 770 cm^{-1} (a″), 598 cm^{-1} (a′), and 501 cm^{-1} (a″) in B_{37}^{3-} (**II**) are all basically maintained in $Ca@B_{37}^{-}$ (**I**), with one extra peak at 239 cm^{-1} (a″) in the latter. The major Raman features at 1256 cm^{-1} (a′), 1206 cm^{-1} (a′), 834 cm^{-1} (a′), 595 cm^{-1} (a′), and 323 cm^{-1} (a′) in **II** are also present in **I**. The breathing modes at 157 cm^{-1} in **II** and 203 cm^{-1} (a′) in **I** belong to typical "radial breathing modes" (RBMs) of the B_{37}^{3-} borospherene cage, with obvious blue shifts from **II** to **I** due to a metal-stabilization effect in the latter. A strong RBM band at 210 cm^{-1} was used to identify the hollow structures of the single-walled boron nanotubes.[47]

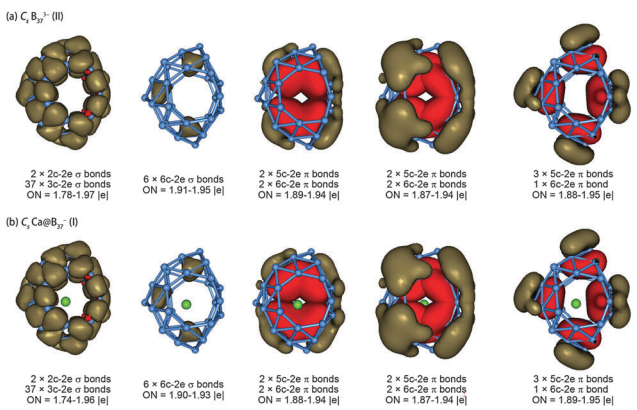

Fig. 2 Comparison of the AdNDP bonding patterns of C_s B_{37}^{3-} (**II**) and C_s $Ca@B_{37}^{-}$ (**I**).

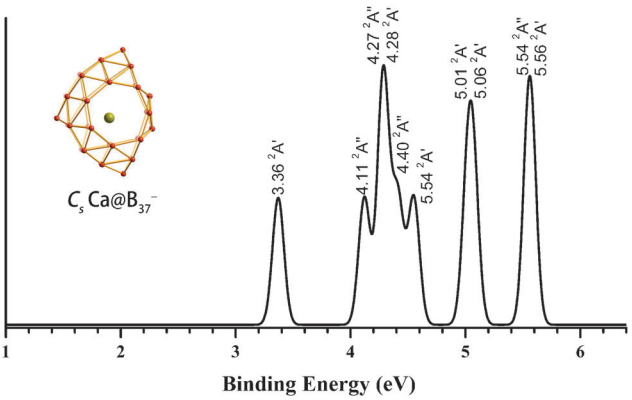

Fig. 4 Simulated PES spectrum of C_s $Ca@B_{37}^{-}$ (**I**) at the TD-PBE0 level.

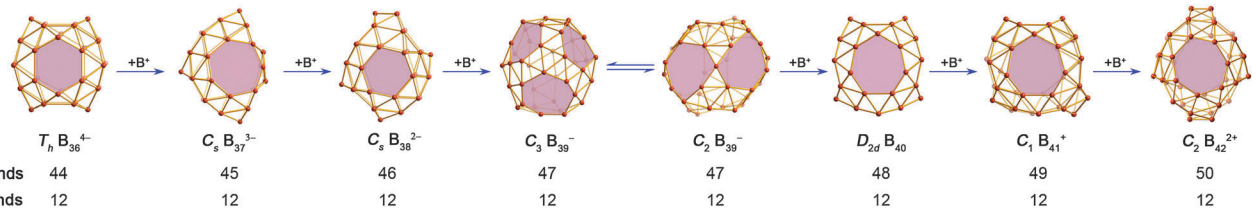

Fig. 5 The B_n^q borospherene family ($q = n - 40$, $n = 36$–42) built up by successively adding a B^+ monocation to the system, starting from the perfect cubic-box-like T_h B_{36}^{4-}. The number of σ and π bonds is indicated for each borospherene cluster.

A combination of anionic PES spectra and first-principles theory calculations has proven to be the most powerful approach to characterize novel boron clusters in the gas phase over the past decade.[8–20,24,26,31] We calculate the vertical excitation energies and simulate the PES spectra of $Ca@B_{37}^-$ (**I**) in Fig. 4 using a time-dependent DFT method.[48] $Ca@B_{37}^-$ (**I**) turns out to have a simulated PES spectrum similar to that of the experimentally observed C_3/C_2 B_{39}^-,[26] with a high first vertical detachment energy of VDE = 3.36 eV. As discussed above, the closed-shell C_s $Ca@B_{37}^-$ (**I**) is π-isovalent with C_3/C_2 B_{39}^- in electronic configurations with a low-lying π-HOMO, resulting in a high VDE for the monoanion. The higher binding-energy bands from 4.0–6.0 eV may serve as fingerprints to characterize $Ca@B_{37}^-$ (**I**) in future experiments. The slightly distorted second lowest-lying isomer C_1 $Ca@B_{37}^-$ (**2**) possesses a similar simulated PES spectrum to C_s $Ca@B_{37}^-$ (**I**), with a first VDE of 3.66 eV (Fig. S2, ESI†). The two lowest-lying isomers may coexist in PES measurements.

In summary, we have presented in this work the possibility of the charge-transfer complex $Ca@B_{37}^-$ (**I**) which contains a metal-stabilized fullerene-like C_s B_{37}^{3-} trianion (**II**) composed of interwoven BDCs with twelve delocalized multicenter π bonds over a σ skeleton, completing the B_n^q borospherene family ($q = n - 40$) in the size range of n = 36–42. As collectively shown in Fig. 5, these borospherenes can be obtained by successively adding a B^+ monocation to the system to form one more σ bond, starting from the perfect fullerene-like T_h B_{36}^{4-}. They are all composed of 12 interwoven BDCs (except C_2 B_{39}^- which possesses a tetracoordinate defect site between two neighboring heptagons[26]) with six pentagonal, hexagonal, or heptagonal faces, analogous to cubane (C_8H_8).[26] More interestingly, they all follow the electronic count of 12 delocalized π bonds over a σ skeleton made of n + 8 σ bonds, giving 3D aromaticity to borospherenes and their derivatives. Considerable research on borospherenes has appeared in the past two years since the discovery of D_{2d} B_{40}, including theoretical predictions of its electronic structure and electronic spectra,[49] topological properties,[50] transition metal complexes $M@B_{40}$ (M = Sc, Y, La),[51] dynamic properties at high temperatures,[52] hydrogen storage capacities[53] and the possibility to form an Au–B_{40}–Au rectifier and photodetector.[54] A prediction of the endohedral complexes $M@B_{38}$ (M = Sc, Y, Ti) was also reported recently.[29,55] The borospherene family closely related to the recently discovered borophene nanosheets[34,35] may be further expanded to other size ranges in either bare clusters or their derivatives. Isolation of borospherenes in macroscopic quantities remains to be realized in experiments to significantly enrich the chemistry of borospherenes and related nanomaterials.

Acknowledgements

This work was financially supported by the National Natural Science Foundation of China (21373130, 21573138, and 21473106).

Notes and references

1 H. W. Kroto, J. R. Heath, S. C. O'Brien, R. F. Curl and R. E. Smalley, *Nature*, 1985, **318**, 162–163.
2 M. Monthioux and V. L. Kuznetsov, *Carbon*, 2006, **44**, 1621–1623.
3 K. S. Novoselov, A. K. Geim, S. V. Morozov, D. Jiang, Y. Zhang, S. V. Dubonos, I. V. Grigorieva and A. A. Firsov, *Science*, 2004, **306**, 666–669.
4 S. Bulusu, X. Li, L. S. Wang and X. C. Zeng, *Proc. Natl. Acad. Sci. U. S. A.*, 2006, **103**, 8326–8330.
5 L. F. Cui, X. Huang, L. M. Wang, D. Y. Zubarev, A. I. Boldyrev, J. Li and L. S. Wang, *J. Am. Chem. Soc.*, 2006, **128**, 8390–8391.
6 L. F. Cui, X. Huang, L. M. Wang, J. Li and L. S. Wang, *J. Phys. Chem. A*, 2006, **110**, 10169–10172.
7 F. A. Cotton, G. Wilkinson, C. A. Murillo and M. Bochmann, *Advanced Inorganic Chemistry*, John Wiley & Sons, Inc., 1999, pp. 131–174.
8 H. J. Zhai, A. N. Alexandrova, K. A. Birch, A. I. Boldyrev and L. S. Wang, *Angew. Chem., Int. Ed.*, 2003, **42**, 6004–6008 (*Angew. Chem.*, 2003, **115**, 6186–6190).
9 H. J. Zhai, B. Kiran, J. Li and L. S. Wang, *Nat. Mater.*, 2003, **2**, 827–833.
10 B. Kiran, S. Bulusu, H. J. Zhai, S. Yoo, X. C. Zeng and L. S. Wang, *Proc. Natl. Acad. Sci. U. S. A.*, 2005, **102**, 961–964.
11 A. P. Sergeeva, Z. A. Piazza, C. Romanescu, W. L. Li, A. I. Boldyrev and L. S. Wang, *J. Am. Chem. Soc.*, 2012, **134**, 18065–18073.
12 W. Huang, A. P. Sergeeva, H. J. Zhai, B. B. Averkiev, L. S. Wang and A. I. Boldyrev, *Nat. Chem.*, 2010, **2**, 202–206.
13 I. A. Popov, Z. A. Piazza, W. L. Li, L. S. Wang and A. I. Boldyrev, *J. Chem. Phys.*, 2013, **139**, 144307.
14 E. Oger, N. R. M. Crawford, R. Kelting, P. Weis, M. M. Kappes and R. Ahlrichs, *Angew. Chem., Int. Ed.*, 2007, **46**, 8503–8506 (*Angew. Chem.*, 2007, **119**, 8656–8659).
15 W. L. Li, Y. F. Zhao, H. S. Hu, J. Li and L. S. Wang, *Angew. Chem., Int. Ed.*, 2014, **53**, 5540–5545 (*Angew. Chem.*, 2014, **126**, 5646–5651).

16 Z. A. Piazza, H. S. Hu, W. L. Li, Y. F. Zhao, J. Li and L. S. Wang, *Nat. Commun.*, 2014, **5**, 3113.
17 A. P. Sergeeva, I. A. Popov, Z. A. Piazza, W. L. Li, C. Romanescu, L. S. Wang and A. I. Boldyrev, *Acc. Chem. Res.*, 2014, **47**, 1349–1358.
18 W. L. Li, Q. Chen, W. J. Tian, H. Bai, Y. F. Zhao, H. S. Hu, J. Li, H. J. Zhai, S. D. Li and L. S. Wang, *J. Am. Chem. Soc.*, 2014, **136**, 12257–12260.
19 Q. Chen, G. F. Wei, W. J. Tian, H. Bai, Z. P. Liu, H. J. Zhai and S. D. Li, *Phys. Chem. Chem. Phys.*, 2014, **16**, 18282–18287.
20 W. L. Li, R. Pal, Z. A. Piazza, X. C. Ze ng and L. S. Wang, *J. Chem. Phys.*, 2015, **142**, 204305.
21 N. G. Szwacki, A. Sadrzadeh and B. I. Yakobson, *Phys. Rev. Lett.*, 2007, **98**, 166804.
22 F. Y. Li, P. Jin, D. E. Jiang, L. Wang, S. B. Zhang, J. J. Zhao and Z. F. Chen, *J. Chem. Phys.*, 2012, **136**, 074302.
23 S. Goedecker, W. Hellmann and T. Lenosky, *Phys. Rev. Lett.*, 2005, **95**, 055501.
24 H. J. Zhai, Y. F. Zhao, W. L. Li, Q. Chen, H. Bai, H. S. Hu, Z. A. Piazza, W. J. Tian, H. G. Lu, Y. B. Wu, Y. W. Mu, G. F. Wei, Z. P. Liu, J. Li, S. D. Li and L. S. Wang, *Nat. Chem.*, 2014, **6**, 727–731.
25 H. Bai, Q. Chen, H. J. Zhai and S. D. Li, *Angew. Chem., Int. Ed.*, 2015, **54**, 941–945.
26 Q. Chen, W. L. Li, Y. F. Zhao, S. Y. Zhang, H. S. Hu, H. Bai, H. R. Li, W. J. Tian, H. G. Lu, H. J. Zhai, S. D. Li, J. Li and L. S. Wang, *ACS Nano*, 2015, **9**, 754–760.
27 Q. Chen, S. Y. Zhang, H. Bai, W. J. Tian, T. Gao, H. R. Li, C. Q. Miao, Y. W. Mu, H. G. Lu, H. J. Zhai and S. D. Li, *Angew. Chem., Int. Ed.*, 2015, **54**, 8160–8164.
28 Q. Chen, T. Gao, W. J. Tian, H. Bai, S. Y. Zhang, H. R. Li, C. Q. Miao, Y. W. Mu, H. G. Lu, H. J. Zhai and S. D. Li, *Phys. Chem. Chem. Phys.*, 2015, **17**, 19690–19694.
29 Q. Chen, H. R. Li, C. Q. Miao, Y. J. Wang, H. G. Lu, Y. W. Mu, G. M. Ren, H. J. Zhai and S. D. Li, *Phys. Chem. Chem. Phys.*, 2016, **18**, 11610–11615.
30 W. J. Tian, Q. Chen, H. R. Li, M. Yan, Y. W. Mu, H. G. Lu, H. J. Zhai and S. D. Li, *Phys. Chem. Chem. Phys.*, 2016, **18**, 9922–9926.
31 Y. J. Wang, Y. F. Zhao, W. L. Li, T. Jian, Q. Chen, X. R. You, T. Ou, X. Y. Zhao, H. J. Zhai, S. D. Li, J. Li and L. S. Wang, *J. Chem. Phys.*, 2016, **144**, 064307.
32 T. B. Tai, S. U. Lee and M. T. Nguyen, *Phys. Chem. Chem. Phys.*, 2016, **18**, 11620–11623.
33 T. B. Tai and M. T. Nguyen, *Chem. Commun.*, 2016, **52**, 1653.
34 A. J. Mannix, X. F. Zhou, B. Kiraly, J. D. Wood, D. Alducin, B. D. Myers, X. Liu, B. L. Fisher, U. Santiago, J. R. Guest, M. J. Yacaman, A. Ponce, A. R. Oganov, M. C. Hersam and N. P. Guisinger, *Science*, 2015, **350**, 1513–1516.
35 B. Feng, J. Zhang, Q. Zhong, W. Li, S. Li, H. Li, P. Cheng, S. Meng, L. Chen and K. Wu, *Nat. Chem.*, 2016, DOI: 10.1038/NCHEM.2491.
36 S. Goedecker, W. Hellmann and T. Lenosky, *Phys. Rev. Lett.*, 2005, **95**, 055501.
37 C. Adamo and V. Barone, *J. Chem. Phys.*, 1999, **110**, 6158–6170.
38 R. Krishnan, J. S. Binkley, R. Seeger and J. A. Pople, *J. Chem. Phys.*, 1980, **72**, 650–654.
39 M. J. Frisch, G. W. Trucks, H. B. Schlegel, G. E. Scuseria, M. A. Robb, J. R. Cheeseman, G. Scalmani, V. Barone, B. Mennucci and G. A. Petersson, *et al.*, *Gaussian 09 Revision D.01*, Gaussian Inc., Wallingford, CT, 2010.
40 J. Čížek, *Adv. Chem. Phys.*, 1969, **14**, 35.
41 G. D. Purvis and R. J. Bartlett, *J. Chem. Phys.*, 1982, **76**, 1910.
42 K. Raghavachari, G. W. Trucks, J. A. Pople and M. Head-Gordon, *Chem. Phys. Lett.*, 1989, **157**, 479.
43 (*a*) H. J. Werner, P. J. Knowles, G. Knizia, F. R. Manby and M. Schütz, *Wiley Interdiscip. Rev.: Comput. Mol. Sci.*, 2012, **2**, 242–253; (*b*) H. J. Werner, P. J. Knowles, G. Knizia, F. R. Manby, M. Schütz, *et al.*, *MOLPRO*, version 2012.1, http://www.molpro.net.
44 E. D. Glendening, J. K. Badenhoop, A. E. Reed, J. E. Carpenter, J. A. Bohmann, C. M. Morales and F. Weinhold, *NBO 5.0*, Theoretical Chemistry Institute, University of Wisconsin, Madison, 2001.
45 D. Yu. Zubarev and A. I. Boldyrev, *Phys. Chem. Chem. Phys.*, 2008, **10**, 5207.
46 P. v. R. Schleyer and C. Maerker, *J. Am. Chem. Soc.*, 1996, **118**, 6317.
47 D. Ciuparu, R. F. Klie, Y. Zhu and L. Pfefferle, *J. Phys. Chem. B*, 2004, **108**, 3967–3969.
48 R. Bauernschmitt and R. Ahlrichs, *Chem. Phys. Lett.*, 1996, **256**, 454–464.
49 R. X. He and X. C. Zeng, *Chem. Commun.*, 2015, **51**, 3185–3188.
50 P. Schwerdtfeger, L. N. Wirz and J. Avery, *Wiley Interdiscip. Rev.: Comput. Mol. Sci.*, 2015, **5**, 96–145.
51 P. Jin, Q. Hou, C. Tang and Z. Chen, *Theor. Chem. Acc.*, 2015, **134**, 13–22.
52 G. Martínez-Guajardo, J. L. Cabellos, A. Díaz-Celaya, S. Pan, R. Islas, P. K. Chattaraj, T. Heine and G. Merino, *Sci. Rep.*, 2015, **5**, 11287.
53 H. Dong, T. Hou, S. T. Lee and Y. Li, *Sci. Rep.*, 2015, **5**, 09952.
54 Z. Yang, Y. L. Ji, G. Lan, L. C. Xu, X. Liu and B. Xu, *Solid State Commun.*, 2015, **217**, 38–42.
55 Q. L. Lu, Q. Q. Luo, Y. D. Li and S. G. Huang, *Phys. Chem. Chem. Phys.*, 2015, **17**, 20897–20902.

